



CrossMark
click for updates

Cite this: DOI: 10.1039/c6md00387g

The discovery of a potent series of carboxamide TRPA1 antagonists†‡

D. C. Pryde,^{§*a} B. Marron,^b C. G. West,^b S. Reister,^b G. Amato,^b K. Yoger,^b K. Padilla,^b J. Turner,^c N. A. Swain,^a P. J. Cox,^c S. E. Skerratt,^a T. Ryckmans,^d D. C. Blakemore,^a J. Warmus^e and A. C. Gerlach^b

Received 13th July 2016,
Accepted 17th August 2016

DOI: 10.1039/c6md00387g

www.rsc.org/medchemcomm

A series of potent and selective carboxamide TRPA1 antagonists were identified by a high throughput screen. Structure–activity relationship studies around this series are described, resulting in a highly potent example of the series. Pharmacokinetic and skin flux data are presented for this compound. Efficacy was observed in a topical cinnamaldehyde flare study, providing a topical proof of pharmacology for this mechanism. These data suggest TRPA1 antagonism could be a viable mechanism to treat topical conditions such as atopic dermatitis.

Introduction

The transient receptor potential (TRP) family of ion channels is comprised of 28 distinct channels, many of which have been implicated as drug targets for a variety of diseases. Substantial literature supports the involvement of these channels in the pathophysiology of pain, inflammatory bowel disease, as well as disorders of the kidney, bladder, skin, respiratory and cardiovascular system.^{1,2}

TRPA1 is the sole member of the TRPA subfamily, a non-selective cation channel expressed in nociceptive dorsal root neurons and visceral tissue that functions as a polymodal sensory receptor and contributes to inflammatory pain signaling.³ The channel is activated by a diversity of inflammatory mediators such as prostaglandin metabolites, Ca²⁺, cold temperatures, 4-hydroxynonenol, allyl isothiocyanate (AITC) and H₂O₂ to produce a generator potential for action potential firing.⁴ Furthermore, TRPA1 channels are expressed at

the pre-synaptic terminals at the level of the spinal cord dorsal horn and may more directly modulate synaptic release and plasticity.⁵ In humans, a gain of function TRPA1 mutation is linked to familial episodic pain syndrome, a severe debilitating pain condition.⁶

Supporting evidence for a role of TRPA1 in pain is provided by selective small molecule TRPA1 inhibitors that are active in both *in vivo* electrophysiological and behavioral pain models.⁷ These include pre-clinical rodent models of induced pain, diabetic peripheral neuropathy, visceral pain and pancreatitis pain. TRPA1 knockout mice are less sensitive to inflammatory pain conditions primarily when measured by mechanical endpoints.⁸

Emerging data also suggests a key role for this channel in mediating itch, particularly itch signaled *via* non-histaminergic pathways that are thought to underpin chronic itch associated with conditions such as atopic dermatitis.⁹ Pruritogens, such as chloroquine and BAM8-22,^{9b} which activate MrgprA3 and MrgprC11 G-protein coupled receptors respectively, have significantly attenuated pruritogenic potential in TRPA1 knockout mice. TRPA1 is pivotal in thymic stromal lymphopoietin, IL-31- and endothelin-induced itch, which are key mediators of itch in atopic dermatitis.¹⁰ Therefore, small molecule TRPA1 inhibitors are hypothesized to have utility in treating conditions in which chronic pain and/or itch are significant symptoms.

TRPA1 has a tetrameric structure that defines a single transmembrane pore region and a very long ankyrin repeat domain in the N-terminal region. The structure of a TRPA1 channel was initially reported at 16 Å resolution using cryo-EM methods,¹¹ which has been followed by a more recent higher resolution structure at approximately 4 Å resolution,¹² although a detailed understanding of how the channel gates

^a Pfizer Worldwide Medicinal Chemistry, Neuroscience and Pain Research Unit, Portway Building, Granta Park, Great Abington, Cambridgeshire, CB21 6GS, UK

^b IcaGen, Inc., 4222 Emperor Boulevard, Suite 350, Durham, North Carolina, NC27703, USA

^c Neuroscience and Pain Research Unit, Portway Building, Granta Park, Great Abington, Cambridgeshire, CB21 6GS, UK

^d Pfizer Worldwide Medicinal Chemistry, Ramsgate Road, Sandwich, Kent, CT13 9NJ, UK

^e Pfizer Worldwide Medicinal Chemistry, Neuroscience and Pain Research Unit, Groton, CT, USA

† All authors are either current or former employees of Pfizer.

‡ Electronic supplementary information (ESI) available: *In vitro* and *in vivo* activity charts, selectivity data and metabolite ID studies for selected compounds. See DOI: 10.1039/c6md00387g

§ Current address: Curadev UK, Innovation House, Discovery Park, Sandwich, Kent, CT14 9FF. E-mail: david@curadev.co.uk

and functions is still lacking. For example, TRPA1 is covalently activated by many reactive and/or noxious substances, which have been proposed to react with the many cysteine residues towards the N-terminus of the protein,¹³ but it is not clear how covalent modifications in this region can be transmitted to gating changes in the pore domain.

Recently, several groups have studied potential binding sites of common TRPA1 ligands¹⁴ many of which are proposed to bind to the menthol binding site based on site-directed mutagenesis data. A number of different small molecule chemotypes with activity at the TRPA1 channel have been reported in the literature¹⁵ and several of these have progressed to human clinical trials.¹⁶ A selection of these chemotypes 1–7 are shown in Fig. 1. We describe here our own efforts to identify and develop a potent and selective series of TRPA1 antagonists starting from a high throughput screening hit.

Results

Screening hit

Our screening was initially based on a high throughput FLIPR assay, which identified actives and were then confirmed using a stable medium throughput electrophysiology assay on the PatchXpress platform. The data presented below in the tables are all confirmed PatchXpress data except where stated. For selected compounds we also tested passive membrane permeability as RRCK permeability¹⁷ and human hepatic microsome stability¹⁸ on selected compounds as a general indication of compound quality.

A high throughput FLIPR screen of the corporate compound collection identified several hit series, the most promising of which was based on a piperidine amide scaffold 8 shown in Fig. 2. This compound showed good potency in the initial FLIPR assay, and when confirmed in the PatchXpress assay showed significantly higher potency with an IC₅₀ of 17 nM. At this stage, we did have some concerns

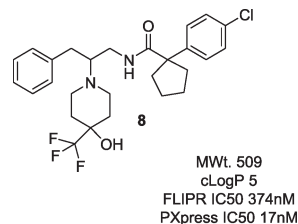


Fig. 2 File screening hit, identified using a FLIPR assay and confirmed in PatchXpress electrophysiology.

about the high lipophilicity of the hit (clogP 5.0), and how dependent on this high lipophilicity potency in the series might be.

However, when further profiled in a broad panel of 132 ion channels, transporters, receptors and enzymes, 8 showed excellent selectivity. When profiled against the other TRP family members implicated in pain, it also showed complete selectivity over the TRPV1 and TRPM8 channels. The synthesis of this compound was short and efficient, and we were able to develop a very straightforward synthesis of compounds from this series as described in the Experimental section below.

Core changes

We screened some close analogues of the initial hit 8 from our compound collection to build early SAR as shown in Table 1.

Piperazine analogues were not active, either in a more polar template 13, or a more lipophilic substituted piperazine scaffold 9. Truncating the left hand side phenyl ring down to the smaller isopropyl group 10 also lost activity, as did capping the amide grouping with a methyl group (14) or replacing the benzyl group with more polar heterocyclic systems 12 and 11. At this stage we also confirmed that 8 had very poor metabolic stability and low permeability in the RRCK assay which was, for the most part, replicated across the analogues depicted in Table 1.

Piperidinol unit and stereoselectivity

These initial SAR findings suggested that large improvements in the metabolic stability or physicochemical properties of the initial lead would be challenging, with significant structural changes around the piperidine ring poorly tolerated. However, improving metabolic stability in the series now became a major area of focus for the project to indicate the future potential of the chemotype to provide an orally available compound. To further explore these observations, several more analogues were designed around a downsized right hand side template which featured a cyclopropyl ring in the benzylic position as a less lipophilic core structure (Table 2). The downsized system 15 was somewhat weaker than its cyclopentyl counterpart 8, but was 1 log unit less lipophilic. Contracting the benzyl substituent to a phenyl substituent 16 further reduced lipophilicity, but ablated activity. Separating the individual enantiomers of the benzylic analogue revealed that most of the activity resided in the *R* enantiomer 18, with the *S* isomer 17 being some 10 fold less active. The more

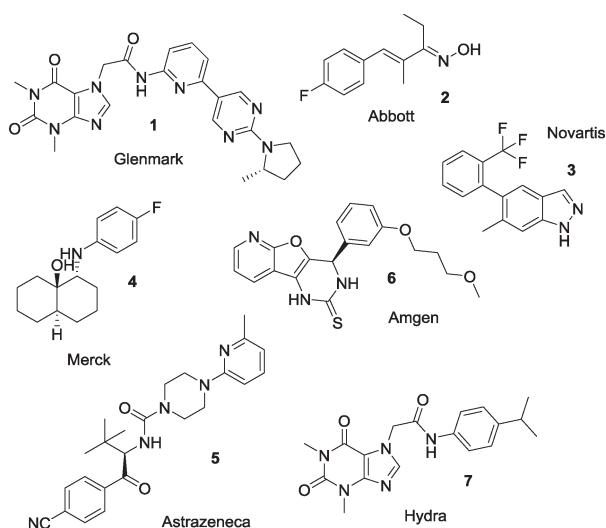


Fig. 1 Examples of chemotypes with reported activity at TRPA1.

Table 1 Early SAR of the primary screening hit

| Comp | R ¹ | R ² | MWt. (clogP) | TRPA1 IC ₅₀ ^a (nM) | HLM (μL min ⁻¹ mg ⁻¹) | RRCK (× 10 ⁻⁶ cm s ⁻¹) |
|------|----------------|----------------|--------------|--|--|---|
| 8 | | H | 509 (5.0) | 17 | >320 | 1 |
| 9 | | H | 503 (6.3) | >1000 | 312 | <1 |
| 10 | | H | 461 (4.5) | >1000 | >320 | <1 |
| 11 | | H | 530.1 (4.2) | 26 700 | 42 | 1 |
| 12 | | H | 517.0 (3.7) | 1900 | >320 | 3 |
| 13 | | H | 440 (4.4) | >3000 | >320 | 3 |
| 14 | | Me | 523 (5.5) | >1000 | >320 | ND |

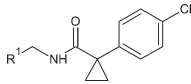
^a PX electrophysiology IC₅₀. All compounds were racemic.

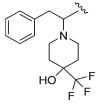
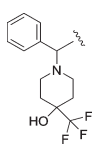
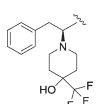
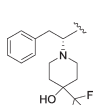
active *R* enantiomer had TRPA1 potency of around IC₅₀ 50 nM, although its metabolic stability was still very poor.

It was of concern that all of the compounds in Table 2, despite reductions in global lipophilicity, all continued to show rapid metabolic turnover in human hepatic microsomes. Metabolite identification studies¹⁹ with **8** showed that compounds within this series were being oxidised in several

places around the molecule. The major metabolites resulted from dehydration and aromatisation of the piperidine ring or oxidations around the amide group and its substituents. These data indicated a need to further overall reduce the global lipophilicity of the series to improve the probability of achieving metabolic stability and to seek more metabolically robust replacements of the piperidine unit.

Table 2 Piperidinol and benzyl variations of the hit compound



| Comp | R ¹ | Stereo-centre ^a | MWt. (clogP) | TRPA1 IC ₅₀ ^a (nM) | HLM (μL min ⁻¹ mg ⁻¹) | RRCK (× 10 ⁻⁶ cm s ⁻¹) |
|------|---|----------------------------|--------------|--|--|---|
| 15 |  | <i>rac</i> | 481 (3.9) | 73 | >320 | 2 |
| 16 |  | <i>rac</i> | 467 (3.6) | >3000 | >320 | 4 |
| 17 |  | <i>S</i> | 481 (3.9) | 474 | >320 | ND |
| 18 |  | <i>R</i> | 481 (3.9) | 53 | >320 | ND |

^a PX electrophysiology IC₅₀. *rac* indicates compounds were racemic.

Amide substituent

Retaining the benzylic left hand side group, we next explored SAR around the right hand side amide substituent with a view to reducing lipophilicity. It was immediately apparent (Table 3) that there was more toleration of structural changes in this region, with TRPA1 activity apparent in structures that featured heteroaromatic (20 and 28), carbocyclic (19, 21, 23) and aliphatic (25, 26, 27) substituents, many with clogP below 4.

We confirmed once more in the hexyl pair of substituents 25 and 26 that most of the activity resided in the *R* enantiomeric series. It was also apparent that bulky and lipophilic substituents such as that in 24 did not guarantee activity and in fact could be detrimental to potency as was also the case with the di-substituted oxazole 22. We tested a selection of compounds from the heterocyclic and alkyl chemotypes for metabolic stability and found them all uniformly to possess poor stability, despite in many cases much reduced lipophilicity.

In the next set of targets we sought to address the metabolic liability of the piperidine unit.

Piperidine analogues

At this point, we incorporated our structure–activity data to date into a set of targets that sought to explore the piperidine

group more fully with various right hand side spiro-fusions and phenyl substitutions in place (Table 4). Simple deletion of the hydroxyl group from the piperidine 29 lost activity compared to the alcohol equivalent 8, as did the ring contracted pyrrolidine 30 and the tropane system 37. Deleting the hydroxyl from the pyrrolidine core then gave a further 5 fold loss in potency 31.

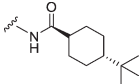
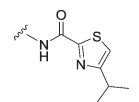
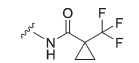
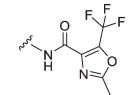
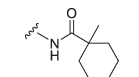
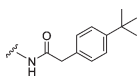
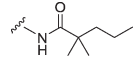
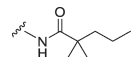
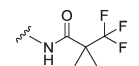
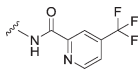
Interestingly, all other changes examined led to a complete loss in activity, including a spiro-fused oxetane 32, spiro-fused cyclopropane 33, bridged piperidine 34 and spiro-fused lactam 36. It was also interesting that deletion of the trifluoromethyl group from the pyrrolidine core in 35 led to a complete loss of activity. Each of these changes had increased the basic pK_a of the central N atom from around pK_a ~6 with up to almost pK_a ~8 with some of these latter changes²⁰ and it is possible that more basic groups which are more ionised at neutral pH's are poorly tolerated at the TRPA1 channel.

Tool compound identification

The SAR we had developed to this point had showed how sensitive the series was to significant structural changes and lipophilicity reduction. Furthermore, in seeking a suitable tool compound for further probing of the pharmacology of

Table 3 Amide analogues of the lead series



| Comp | R ¹ | Stereo-centre ^a | MWt (clog <i>P</i>) | TRPA1 IC ₅₀ ^a (nM) | HLM (μL min ⁻¹ mg ⁻¹) | RRCK (× 10 ⁻⁶ cm s ⁻¹) |
|------|---|----------------------------|----------------------|--|--|---|
| 19 |  | <i>rac</i> | 468.3 (5.1) | 101 | >320 | ND |
| 20 |  | <i>rac</i> | 455.2 (3.8) | 159 | >320 | ND |
| 21 |  | <i>rac</i> | 438.2 (2.1) | 1000 | 149 | ND |
| 22 |  | <i>rac</i> | 479.2 (1.8) | >10 000 ^b | 146 | ND |
| 23 |  | <i>rac</i> | 426.2 (3.8) | 851 | >320 | ND |
| 24 |  | <i>rac</i> | 476.3 (4.8) | >10 000 ^b | >320 | ND |
| 25 |  | <i>S</i> | 414.5 (3.5) | 1700 ^b | ND | ND |
| 26 |  | <i>R</i> | 414.5 (3.5) | 71 ^b | ND | ND |
| 27 |  | <i>rac</i> | 440.2 (2.6) | 91 | 284 | 31 |
| 28 |  | <i>rac</i> | 493.2 (3.6) | 83 | 285 | 8 |

^a PX electrophysiology IC₅₀. *rac* indicates compounds were racemic. ^b FLIPR IC₅₀.

TRPA1 we had not identified a metabolically stable compound suitable for oral dosing. However, we had identified a number of potent and selective TRPA1 antagonists, and returned to the original early screening hit 8 to work this up into a tool compound for further evaluation of the target.

The enantiomers were separated and again showed that the major activity resided in the *R* enantiomer 39 (Fig. 3).

When tested in single rig electrophysiology, 39 showed excellent potency of IC₅₀ < 1 nM, and demonstrated potent activity across several species of TRPA1, albeit

Table 4 Piperidine variations

| Comp | R ₁ | R ₂ | R ₃ /R ₄ | MWt (clog <i>P</i>) | TRPA1 IC ₅₀ ^a (nM) | HLM (μL min ⁻¹ mg ⁻¹) | RRCK (× 10 ⁻⁶ cm s ⁻¹) |
|------|----------------|----------------|--------------------------------|----------------------|--|--|---|
| 29 | H | | | 492.2 (6.5) | 673 | 238 | 6 |
| 30 | H | | | 464.2 (4.6) | 309 | ND | ND |
| 31 | F | | | 480.2 (5.8) | 1451 | ND | ND |
| 32 | F | | | 468.3 (4.6) | >10 000 ^b | >320 | ND |
| 33 | F | | | 474.2 (5.2) | >10 000 ^b | >320 | 0.3 |
| 34 | F | | | 427.0 (5.3) | >10 000 ^b | >320 | ND |
| 35 | F | | | 428.5 (4.2) | >10 000 ^b | 170 | ND |
| 36 | F | | | 484.0 (3.2) | >10 000 ^b | 168 | ND |
| 37 | F | | | 536.6 (4.9) | 825 | >320 | ND |

All compounds were racemic.^a PX electrophysiology IC₅₀.^b FLIPR IC₅₀.

somewhat less potent at the pig channel (Fig. 4). It showed high turnover in hepatic microsomes, low perme-

ability, low aqueous solubility and high plasma stability indicating there to be no amide hydrolysis contributing to

the degradation of the compound during the metabolism assays.

It showed excellent selectivity in a broad panel of 112 screens and no genetic toxicity flags. **39** showed no activity at either the TRPM8 or the TRPV1 channels. Overall, this compound represented an excellent tool compound to further explore TRPA1 pharmacology.

Binding site elucidation

As mentioned above, there has been an increase in literature activity recently in trying to elucidate the binding sites of small molecule ligands of the TRPA1 channel. Most publications have centred on a region around S5 that has been shown to affect the binding of menthol, and related terpene molecules, centred around the S873 and T874 residues.¹⁴ This suggests that the channel can be modulated through binding either to the N-terminal region which is rich in cysteine residues, or to this S5 region.

In order to generate some hypotheses of where our tool compound series was binding to the TRPA1 channel, we generated several ortholog chimeras based on hTRPA1 and the opossum version of the channel (oTRPA1) due to its diversity of sequence in the pore region. Chimeras were made in which the S5 region of the two ortholog species were swapped, as shown in Fig. 5.

Using these reagents, the activity of **39** was investigated as shown in Fig. 6. **39** was most potent against the hTRPA1 channel, but lost almost all activity when the S5 region was swapped to that of the opossum sequence. **39** had almost no activity against oTRPA1, but to a large extent its activity was rescued by insertion of the human S5 sequence.

Together, these data indicated the importance of the S5 region of the channel for the bioactivity of the series.

Topical flare study

At this point in the project we had identified a potent and selective series and demonstrated using computational and mutation studies that the series bound in the menthol binding site region of S5 but we had been unable to increase metabolic stability to the extent that it could be considered a useful oral series. We were aware of the extensive literature that had been published on the role of TRPA1 in topical conditions including itch²¹ and chronic cough²² as a chemosensor

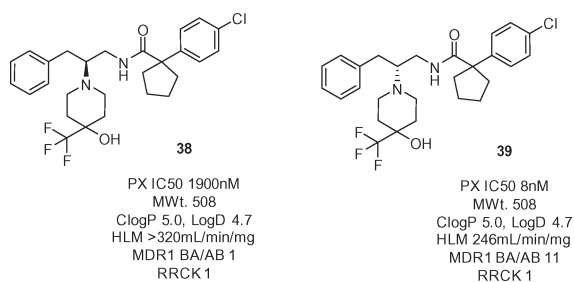


Fig. 3 Separated enantiomers of **8**.

MWt. 509, LogD 5.0
TPSA 53, pKa 5.9
Human TRPA1 PX IC₅₀ 8 nM
Human single rig EP IC₅₀ 0.7 nM
Rat TRPA1 single rig IC₅₀ 3 nM
Mouse TRPA1 single rig IC₅₀ 4 nM
Pig TRPA1 single rig IC₅₀ 65 nM

AMES –ve, IVMN –ve
Cardiac panel > 3000 nM (Kv1.5, Nav1.5, LQT1)
Dofetilide binding K_i 25700 nM
hERG IC₅₀ > 3 μM
TRPM8 IC₅₀ > 3 μM
TRPV1 IC₅₀ > 3 μM
Broad ligand/kinase/PDE panel IC₅₀ > 3 μM,
except for GABAA (Cl channel) IC₅₀ 2.3 μM and
Na site 2 IC₅₀ 730 nM

HLM 246, hHep 38 mL/min/mg
RLM 524, Rhesp 30 mL/min/mg
Plasma stability:
Dog > 360 min, Rat > 360 min
RRCK 1, MDCK 1/11
Kinetic solubility (pH 6.5) 12 μM
Thermodynamic solubility 0.6 μg/mL
Human fu 0.0011, dog 0.0008, rat 0.00057

CYP1A2 IC₅₀ > 30000 nM
CYP2C19 IC₅₀ 3152 nM
CYP2C8 IC₅₀ 11781 nM
CYP2C9 IC₅₀ 11405 nM
CYP3A4 IC₅₀ 2164 nM
CYP2D6 IC₅₀ 450 nM

Fig. 4 Further profile data for compound **39**.

for environmental irritants. In these conditions, effective agents would be efficacious at the local site of administration and not require a long systemic pharmacokinetic half-life.

The rat pharmacokinetics of **39** were measured and showed moderate to high clearance and low oral bioavailability (clearance 42 ml min⁻¹ kg⁻¹, V_{dss} 3.99 L kg⁻¹, T_{1/2} 4.4 h, F 5%). The systemic pharmacokinetics of **39** following a topically applied dose of compound were also examined in the rat. A dose of 0.68 mg per animal was given using a 27 mg mL⁻¹ solution of **39** in 70% ethanol/30% polyethyleneglycol applied to a 5 cm² area of skin and systemic levels of **39** monitored for 24 hours. At all time points the levels of compound observed were low, and well below IC₅₀ concentrations. Indeed at most of the time points compound levels were below the limit of quantitation in the bioanalysis assay. We examined the skin flux properties of the compound which showed low skin permeability (0.1 × 10⁻⁵ cm h⁻¹) but high concentrations in both the epidermal layer (3128 μg g⁻¹) and in the dermal layer (640 μg g⁻¹) following topical administration, confirming the compound had good skin retention properties.

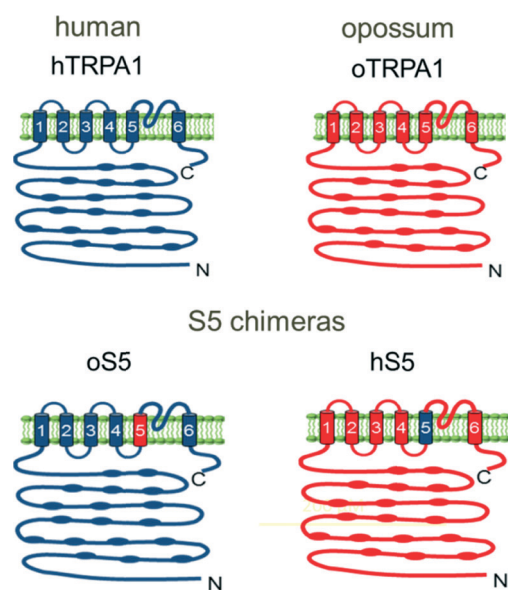


Fig. 5 Design of the hTRPA1 and oTRPA1 ortholog chimeras.

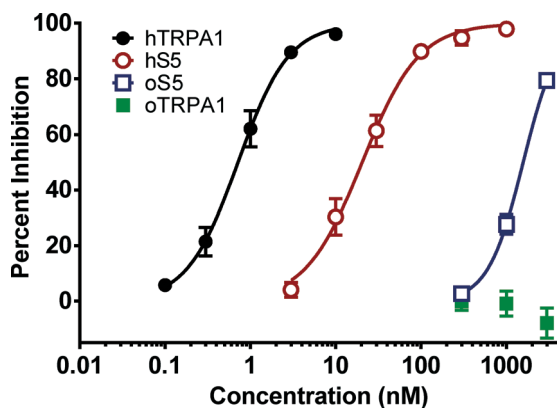


Fig. 6 Carboxamide **39** potency is dependent on the TRPA1 S5 helix. TRPA1 species ortholog chimeras were generated to identify the critical region of interaction, stably expressed in hEK293 cells and evaluated using whole-cell voltage clamp electrophysiology. Opossum TRPA1 (oTRPA1) was selected as the human (hTRPA1) chimeric partner because of divergence in the channel pore region (68% identity in S5–S6) hTRPA1/oTRPA1 chimeras were generated by swapping the 27 amino acid comprising S5. hS5 designates chimeras in which hTRPA1 amino acids 867–893 were swapped into oTRPA1. oS5 designates chimeras in which oTRPA1 amino acids 870–896 were swapped into hTRPA1. The mean IC_{50} (95% confidence interval, n) was (●) hTRPA1 = 0.72 nM (95% CI = 0.60–0.85 nM, n = 6), (○) hS5 = 20 nM (95% CI = 17–25 nM, n = 5), (□) oS5 = 1578 nM (95% CI = 1426–1745 nM, n = 4) and (■) oTRPA1 \geq 3000 nM (n = 4).

We designed a topical flare study in the rat, in which test compound was formulated in vehicle, applied to the skin and left for a defined period of time. After this time, a 20% v/v formulation of cinnamaldehyde in the study vehicle was then applied to the same location and blood flow measured in the dosed region by laser Doppler sonography. The test compound chosen for this initial study was the racemate **8**. Responses were compared directly to an example of a literature TRPA1 antagonist, for which we chose compound **4** as a small molecule analogue of similar lipophilicity and *in vitro* potency to **8** (compound **4** showed human TRPA1 PX IC_{50} 10 nM and rat TRPA1 PX IC_{50} 8 nM in our hands). This compound also offered a useful comparator as our data suggested it to have a higher skin flux of 8×10^{-5} cm h^{-1} , but lower concentrations retained in both the dermis (232 μg g^{-1}) and epidermis (86 μg g^{-1}) compared to **8** for an equivalent administered dose. Typically, the literature²³ would suggest that for effective transdermal delivery of compounds, they should be low molecular weight (<400) and moderately polar ($\log P < 4$), which was consistent with the properties of **4** and our skin flux data findings, and provided an excellent contrasting profile to **8**.

Fig. 7 shows the cinnamaldehyde-induced flare data for **8** at two different concentrations. Systemic pharmacokinetic analysis showed no measurable levels of any compound in the systemic circulation. Skin samples were not analysed due to difficulties extracting meaningful values.

Topically applied **8** significantly reduced cinnamaldehyde-mediated flare in rat skin. Comparing the two dose groups, increasing the concentration of topically applied **8** made no difference to the effect on cinnamaldehyde-induced erythema in rat

skin. At each timepoint, the AUC figures for 50 mg ml^{-1} and 100 mg ml^{-1} doses were very similar and equally effective at reducing cinnamaldehyde-induced flare ($P < 0.01$). Three pre-dose timepoints were examined in this study. Only the 30 min data are shown in Fig. 7. Theoretically, a longer pre-dose time allows the compound time to transition through the outer skin layers and engage with TRPA1 receptors within the skin, but all pre-dose times significantly ($P < 0.01$) reduced cinnamaldehyde-induced flare. However 30 min appeared to be sufficient time for the compound to traverse relatively thin rat skin. Increasing the pre-dose time potentially also allows more time to be lost to metabolic processes in the skin, non-specific protein binding or passing through the skin and being systemically metabolised. Confirming these theories were outwith the scope of these studies.

Comparing these data to those obtained with a 50 mg ml^{-1} dose of **4** (Fig. 8), the two datasets look very similar, despite the diversity of skin flux and retention data displayed by the two compounds. The 60 min pre-dose data is shown in Fig. 8.

Further study is required to identify an optimal skin flux and skin retention compound profile, but these data clearly show that a topically-administered TRPA1 antagonist can ablate an inflammatory flare response.

Conclusions

We have identified potent selective inhibitors of the TRPA1 ion channel based on a carboxamide template. Efforts to enhance the *in vitro* ADME properties of this series with a goal to improve the oral bioavailability of this series, proved futile. However, an exemplar compound from this series accumulated to high levels in skin and engaged with the target, in the absence of significant systemic exposure, when administered topically in rodent CA flare studies. The skin is a major neurosensory organ

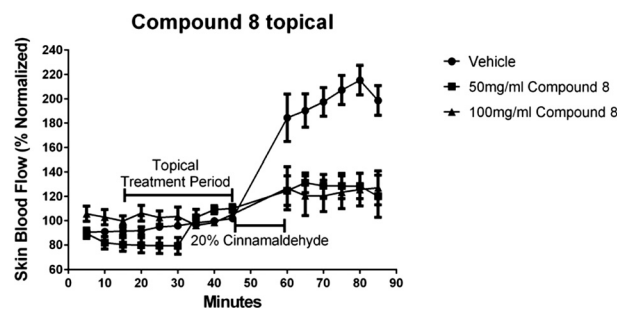


Fig. 7 Normalised flare response to topical *trans*-cinnamaldehyde (20% solution in ethanol) in animals dosed topically with vehicle or the selective TRPA1 blocker **8**, n = 8 per group. Each data point represents mean blood flow in a 5 minute laser Doppler scan over a 2.5 cm^2 scan area. Baseline measurements were taken for 10 minutes before treatment was delivered topically. Laser Doppler scans continued during the pre-treatment then for a further 5 minutes to establish a post-dose baseline. 50 μl of 20% *trans*-cinnamaldehyde solution was administered topically to the centre of the scan area using a 12 mm polypropylene coated aluminium Finn chamber for a 10 minute duration. Doppler scans were not recorded during this period. The Finn chamber was then removed and laser Doppler flowmetry scans were then recorded for 30 minutes.

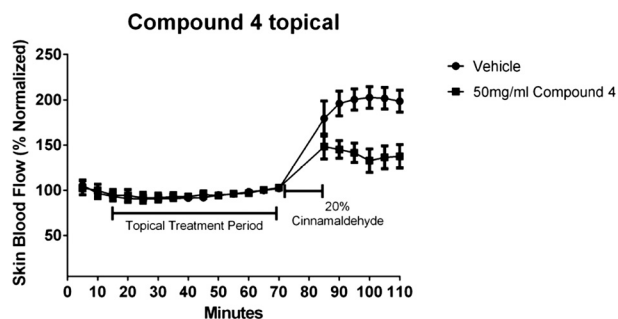


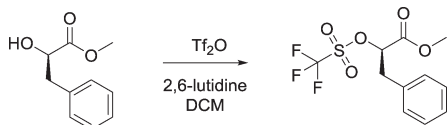
Fig. 8 Normalised flare response to topical *trans*-cinnamaldehyde (20% solution in ethanol) in animals dosed topically with vehicle or the selective TRPA1 blocker **4**, $n = 8$ per group. Experiments were conducted as described for **8**.

where the symptoms of pain and itch in chronic diseases are most often first perceived, therefore we hypothesize that carbamide based inhibitors of TRPA1 could offer potential safe and effective topical treatments for pain or itch.

Experimental

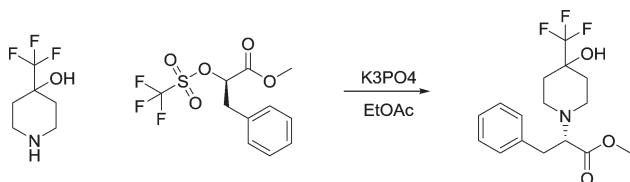
An example of the synthetic routes followed to prepare the compounds contained herein is shown below for compound **39**.

(*R*)-Methyl 3-phenyl-2-(((trifluoromethyl)sulfonyl)oxy)propanoate



To a cooled solution ($-10\text{ }^{\circ}\text{C}$) of (*R*)-methyl 2-hydroxy-3-phenylpropanoate (0.99 g, 5.49 mmol) in DCM (14 mL) was added 2,6-lutidine (0.77 mL, 6.6 mmol) followed by trifluoromethanesulfonyl anhydride (1.11 mL, 6.59 mmol) dropwise. The reaction was stirred at this temperature for 1 hour. The reaction was quenched by the addition of water and stirred for 2 minutes. The solution was extracted into DCM and the organic layer was collected, dried over magnesium sulphate and concentrated *in vacuo*. The residue was purified using silica gel column chromatography eluting with 0–25% EtOAc in heptanes to afford the title compound as an oil (1.435 g, 84%). $^1\text{H NMR}$ (400 MHz, CDCl_3): δ 3.15–3.25 (m, 1H), 3.30–3.40 (m, 1H), 3.85 (s, 3H), 5.10–5.15 (m, 1H), 7.10–7.40 (m, 5H) ppm.

(*S*)-Methyl-2-(4-hydroxy-4-(trifluoromethyl)piperidin-1-yl)-3-phenylpropanoate



To a solution of (*R*)-methyl 3-phenyl-2-(((trifluoromethyl)sulfonyl)oxy)propanoate (3 g, 9.6 mmol) in EtOAc (24.6 mL)

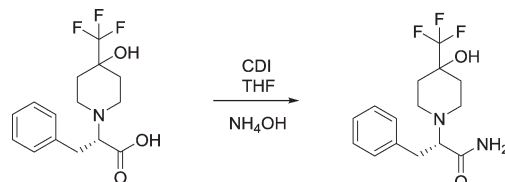
was added 4-(trifluoromethyl)piperidin-4-ol (2.72 g, 9.61 mmol) and potassium phosphate (8.16 g, 38.4 mmol) and the reaction was stirred at room temperature for 18 hours. The reaction was diluted with EtOAc, washed with water, dried over magnesium sulphate and concentrated *in vacuo*. The residue was purified using silica gel column chromatography eluting with 0–25% EtOAc in heptanes to afford the title compound (1.93 g, 60%). **HPLC analysis:** column: XBridge C18 150×4.6 mm, 5 micron; mobile phase A: water with 0.1% TFA, mobile phase B: MeCN with 0.1% TFA. Gradient: 5% B for 0–1.5 min, 5–100% B for 1.5–10 min, 100% B for 10–11 min and 100–5% B for 11–12 min. Flow rate 1.5 mL min^{-1} . $R_t = 5.96$ minutes. $^1\text{H NMR}$ (400 MHz, CDCl_3): δ 1.50–2.00 (m, 4H), 3.05–3.20 (m, 2H), 3.20–3.38 (m, 3H), 3.75 (s, 3H), 3.75–3.85 (m, 1H), 4.40–4.52 (m, 1H), 7.20–7.42 (m, 5H) ppm.

(*S*)-2-(4-Hydroxy-4-(trifluoromethyl)piperidin-1-yl)-3-phenylpropanoic acid



A solution of (*S*)-methyl 2-(4-hydroxy-4-(trifluoromethyl)piperidin-1-yl)-3-phenylpropanoate (1.3 g, 3.924 mmol) in 6 N HCl (aq) (30 mL) was heated to $90\text{ }^{\circ}\text{C}$ for 18 hours. The reaction was cooled to $-10\text{ }^{\circ}\text{C}$ with a brine/ice mixture and treated with 6 N NaOH (aq) until pH = 3–4. The aqueous mixture was extracted into EtOAc four times. The organic layers were combined, washed with brine, dried over sodium sulphate and concentrated *in vacuo* to afford the title compound that was used directly in the next step (1.2 g, 97%). MS m/z 318 $[\text{M} + \text{H}]^+$. $^1\text{H NMR}$ (400 MHz, MeOH-d_4): δ 2.00–2.30 (m, 4H), 3.10–3.30 (m, 2H), 3.40–3.65 (m, 3H), 3.75–3.85 (m, 1H), 4.30–4.50 (m, 1H), 7.25–7.45 (m, 5H) ppm.

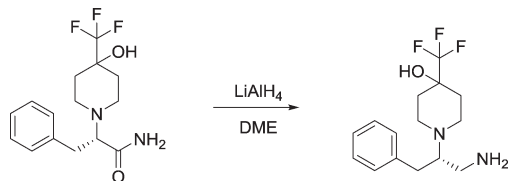
(*S*)-2-(4-Hydroxy-4-(trifluoromethyl)piperidin-1-yl)-3-phenylpropanamide



A solution of (*S*)-2-(4-hydroxy-4-(trifluoromethyl)piperidin-1-yl)-3-phenylpropanoic acid (1211 mg, 3.816 mmol) and carbonyldiimidazole (1180 mg, 7.25 mmol) in THF (38 mL) was stirred at room temperature for 1 hour before cooling to $0\text{ }^{\circ}\text{C}$. Ammonium hydroxide (2.97 mL) dropwise was added and the reaction was stirred at $0\text{ }^{\circ}\text{C}$ for 30 minutes. The reaction was diluted with water and extracted into EtOAc. The organic layer was collected, dried over magnesium sulphate and concentrated *in vacuo*. The residue was purified using

silica gel column chromatography eluting with 0–75% EtOAc in heptanes to afford the title compound (1 g, 83%) as a yellow oil which was used immediately in the next step.

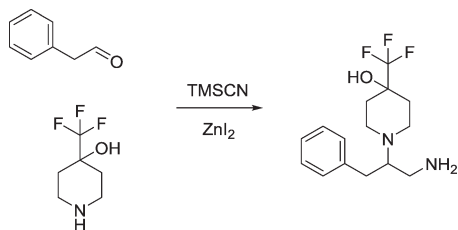
(S)-1-(1-Amino-3-phenylpropan-2-yl)-4-(trifluoromethyl)piperidin-4-ol



To a solution of (S)-2-(4-hydroxy-4-(trifluoromethyl)piperidin-1-yl)-3-phenylpropanamide (919 mg, 2.90 mmol) in THF (14.5 mL) was added a 0.5 M solution of LiAlH₄ in DME (14.5 mL) and the reaction was heated to 65 °C for 6 hours followed by heating at 50 °C for 18 hours. The reaction was cooled to –7 °C and quenched by the addition of water (0.3 mL), followed by 15% (aq) NaOH solution (0.3 mL) followed by water (0.9 mL) and stirred for 1 hour. The reaction was diluted with diethyl ether and filtered through a pad of sodium sulphate. The filtrate was collected and concentrated *in vacuo* to afford the title compound as a white solid (778 mg, 87%). MS *m/z* 303 [M + H]⁺. ¹H NMR (400 MHz, CDCl₃): δ 1.60–1.76 (m, 3H), 1.82–1.92 (m, 1H), 2.21–2.30 (t, 2H), 2.46–2.72 (m, 5H), 2.85–2.99 (m, 2H), 7.08–7.27 (m, 5H) ppm.

A shorter racemic synthesis of this amine was achieved in fewer steps as below.

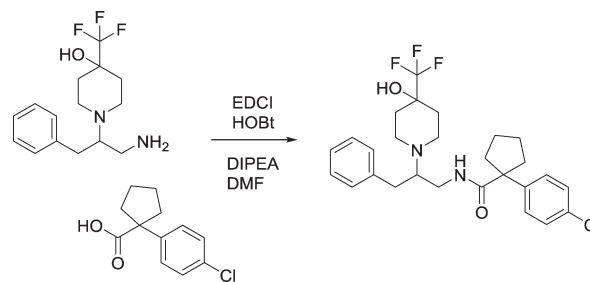
rac-1-(1-Amino-3-phenylpropan-2-yl)-4-(trifluoromethyl)piperidin-4-ol



A solution of phenylacetaldehyde (355 mg, 2.96 mmol) and trimethylsilylcyanide (293 mg, 2.96 mmol) in diethyl ether (1.5 mL) was treated with zinc iodide (5 mg) and stirred at room temperature for 15 minutes. 4-(Trifluoromethyl)piperidin-4-ol (500 mg, 2.96 mmol) in MeOH (5 mL) was added and the reaction heated to reflux for 18 hours. The reaction was cooled and concentrated *in vacuo*, azeotroping with toluene. The residue was dissolved in THF (5 mL), treated with LiAlH₄ (2 M solution in THF, 2.2 mL, 4.43 mmol) and stirred at room temperature for 48 hours. The reaction was diluted with TBME (10 mL) and treated with water (0.17 mL), 15% (aq) NaOH solution (0.17 mL) followed by another aliquot of water (0.51 mL). Sodium sulphate was added and the reaction was filtered and concentrated *in vacuo*. The residue was purified using silica gel column chromatography eluting with DCM:MeOH:NH₃, 90:9:1 to 80:18:2 to afford

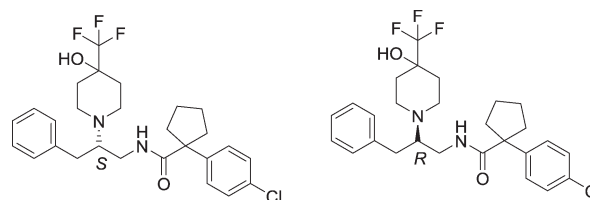
the title compound as a colourless oil (600 mg, 74%). MS *m/z* 303 [M + H]⁺. ¹H NMR (400 MHz, MeOH-d₄): δ 1.75–1.80 (m, 3H), 1.83–1.90 (m, 1H), 2.35–2.50 (m, 2H), 2.55–2.65 (m, 3H), 2.75–2.80 (m, 2H), 2.90–3.03 (m, 2H), 7.15–7.30 (m, 5H) ppm. The enantiomers were then separated using a Chiralpak AD-H. Mobile phase: 30% IPA in heptanes modified with 0.1% DEA in IPA. Flow rate: 18 mL min⁻¹ (preparative); 1 mL min⁻¹ (analytical). (S)-1-(1-Amino-3-phenylpropan-2-yl)-4-(trifluoromethyl)piperidin-4-ol, *R*_t = 3.95 minutes and (R)-1-(1-amino-3-phenylpropan-2-yl)-4-(trifluoromethyl)piperidin-4-ol, *R*_t = 4.95 minutes.

rac-1-(4-Chlorophenyl)-N-{2-[4-hydroxy-4-(trifluoromethyl)piperidin-1-yl]-3-phenylpropyl}cyclopentanecarboxamide



To a solution of *rac*-1-(1-amino-3-phenylpropan-2-yl)-4-(trifluoromethyl)piperidin-4-ol (50 mg, 0.214 mmol) in DMF (1 mL) was added 1-(4-chlorophenyl)cyclopentanecarboxylic acid (37 mg, 0.165 mmol), DIPEA (0.035 mL, 0.198 mmol) and EDCI (38 mg, 0.198 mmol), followed by HOBT (30 mg, 0.198 mmol) and the reaction was stirred at room temperature for 18 hours. Water was added and the reaction stirred for a further 2 hours. DCM was added with further stirring for 1 hour followed by elution through a phase separation cartridge. The organic filtrate was concentrated *in vacuo*. The residue was dissolved in MeOH and treated with ethereal HCl with standing for 18 hours. The resulting suspension was filtered and triturated with EtOAc, heptanes and TBME to afford the title compound as the hydrochloride salt (69 mg, 82%). ¹H NMR (400 MHz, DMSO-d₆): δ ppm 1.50–1.60 (m, 4H), 1.70–1.90 (m, 4H), 2.15–2.25 (m, 2H), 2.40–2.48 (m, 2H), 2.70–2.80 (m, 1H), 3.05–3.25 (m, 6H), 3.47–3.62 (m, 2H), 6.38 (br s, 1H), 7.20–7.40 (m, 9H), 7.80 (br m, 1H). MS *m/z* 509 [M + H]⁺.

(S) and (R)-1-(4-chlorophenyl)-N-{2-[4-hydroxy-4-(trifluoromethyl)piperidin-1-yl]-3-phenylpropyl}cyclopentanecarboxamide



To a suspension of (S)-1-(1-amino-3-phenylpropan-2-yl)-4-(trifluoromethyl)piperidin-4-ol (70 mg, 0.232 mmol) and

1-(4-chlorophenyl)cyclopentanecarboxylic acid (57.3 mg, 0.255 mmol) in acetonitrile (0.8 mL) was added triethylamine (0.133 mL, 0.928 mmol) followed by propylphosphonic anhydride (50% wt solution in EtOAc, 0.21 mL, 0.35 mmol). The reaction was stirred at room temperature for 1.5 hours after which the solution was purified directly by silica gel column chromatography eluting with 0–30% EtOAc in heptanes to afford the title compound (75 mg, 64%). $[\alpha]_D^{20} = +9.6$ in DCM [20 mg mL⁻¹]. ee determination column: ChiralTech AD-H, 250 × 4.6 mm, 5 micron. Mobile phase A: CO₂; mobile phase B: MeOH with 0.2% ammonium hydroxide. Gradient: 5% B at 0.00 min, 60% B at 9.00 min; hold to 9.5 min and return to 5% B at 10 min. Flow rate 3 mL min⁻¹. $R_t = 5.05$ minutes, ee = 95%.

The title compounds may also be prepared from *rac*-1-(4-chlorophenyl)-*N*-{2-[4-hydroxy-4-(trifluoromethyl)piperidin-1-yl]-3-phenylpropyl}cyclopentanecarboxamide prepared as above. The racemate was separated into two enantiomers using preparative chiral chromatography as described below: Chiralpak IA, 4.6 × 250 mm, 5 micron. Mobile phase: hexane:DCM:EtOH:DEA 90:8:2:0.1. Flow rate: 1 mL min⁻¹, $R_t = 8.351$ minutes and $R_t = 10.068$ minutes. The first eluting isomer is (*S*)-1-(4-chlorophenyl)-*N*-{2-[4-hydroxy-4-(trifluoromethyl)piperidin-1-yl]-3-phenylpropyl} cyclopentane-carboxamide, ee = 100%. The second eluting isomer is (*R*)-1-(4-chlorophenyl)-*N*-{2-[4-hydroxy-4-(trifluoromethyl)piperidin-1-yl]-3-phenylpropyl} cyclopentane-carboxamide, ee = 99.62%.

The compounds prepared from the chiral separation method are identical by α -rotation and retention time to the compounds prepared as the single enantiomer described above.

MS *m/z* 509 [M + H]⁺. ¹H NMR (400 MHz, DMSO-*d*₆): δ 1.30–1.80 (m, 10H), 2.20–2.30 (m, 1H), 2.35–2.60 (m, 6H), 2.65–2.85 (m, 4H), 3.00–3.15 (m, 1H), 5.50 (br s, 1H), 6.95–7.00 (m, 1H), 7.05–7.15 (m, 2H), 7.20–7.35 (m, 6H) ppm.

In vivo efficacy studies

All experiments were performed in compliance with the laws and institutional guidelines of the UK Home Office.

8 topical study

Treatment groups. Male Sprague Dawley rats were weighed and randomised to one of the following treatment groups:

Group I: vehicle (5 μ l cm⁻², topical); 30 minute pre-dose.

Group II: 50 mg ml⁻¹ 8 (5 μ l cm⁻², topical); 30 minute pre-dose.

Group III: 100 mg ml⁻¹ 8 (5 μ l cm⁻², topical); 30 minute pre-dose.

Group IV: vehicle (5 μ l cm⁻², topical); 60 minute pre-dose.

Group V: 50 mg ml⁻¹ 8 (5 μ l cm⁻², topical); 60 minute pre-dose.

Group VI: 100 mg ml⁻¹ 8 (5 μ l cm⁻², topical); 60 minute pre-dose.

Group VII: vehicle (5 μ l cm⁻², topical); 90 minute pre-dose.

Group VIII: 50 mg ml⁻¹ 8 (5 μ l cm⁻², topical); 90 minute pre-dose.

Group IX: 100 mg ml⁻¹ 8 (5 μ l cm⁻², topical); 90 minute pre-dose.

Formulation and dosing. 8 was formulated into a solution of 70:30 ethanol:propylene glycol and dosed at 6 μ l cm⁻². To a weighing of the compound (equivalent to a final concentration of 50 or 100 mg mL⁻¹), ethanol was added to 70% of the final volume. This was sonicated until dissolved, prior to addition of 30% of final volume of propylene glycol. This was mixed well to give a final clear solution for dosing. *trans*-Cinnamaldehyde (99%, Sigma-Aldrich, Munich, Germany) was dissolved in 100% ethanol at 20% v/v and dosed topically at 50 μ l dose volume.

Laser Doppler imaging protocol. Male Sprague Dawley rats were weighed and randomised to one of 2 treatment groups, placed in an anaesthetic chamber and anaesthetized with a 5% isoflurane/O₂ mix. Animals were then moved to a homoeothermic heat mat and anaesthesia maintained at approximately 2% isoflurane/O₂ during the laser Doppler scanning *via* nose cone for the duration of the study. The abdomen was then shaved to allow laser Doppler flowmetry scans to be taken over an approximate area of 2.5 cm². Baseline scans were recorded for 10 min, subsequently 15 μ l of compound or vehicle (70:30 ethanol:propylene glycol) was then applied to the centre of the scan area. The treatment was left to penetrate the skin for 30–90 minutes while baseline blood flow was measured. After the treatment period, a further 5 post-dose Doppler scans were completed to establish a post-dose baseline before 50 μ l of 20% *trans*-cinnamaldehyde (99%, Sigma-Aldrich, Munich, Germany) dissolved in 100% ethanol was administered topically to the centre of the scan area using a 12 mm polypropylene coated aluminium Finn chamber on Scanpor tape (Biodiagnostics Ltd, Worcestershire) applied for a 10 minute duration. The Finn chamber was removed and laser Doppler flowmetry scans were then recorded for 30 minutes. In all cases, the operator was blinded to treatment identity.

Sample collection schedule. Terminal PK samples were taken from all animals *via* cardiac puncture at study endpoint (70–150 min post topical dose depending on pre-dose time). Blood samples were centrifuged and resultant plasma samples were frozen at –20 °C prior to bioanalysis.

Equipment and supplies list. MoorLDI2 laser Doppler imager (Moor Instruments Ltd, Axminster, UK).

Data analysis. All data design, randomization and analysis were handled in accordance with previous discussions with the Non-Clinical Statistics group. In brief, area under the curve (AUC) analysis was carried out for normalized blood flow following cinnamaldehyde challenge. AUC values were then compared across groups using one-way ANOVA.

4 topical study

Treatment groups. Male Sprague Dawley rats were weighed and randomised to one of the following treatment groups, *N* = 8 per group:

Group I: vehicle (6 μ l cm⁻², topical); 60 minute pre-dose.

Group II: 4 (50 mg ml⁻¹, 6 μ l cm⁻², topical); 60 minute pre-dose.

The above treatment groups were dosed prior to *trans*-cinnamaldehyde application.

Formulation and dosing. 4 was formulated into a solution of 70:30 ethanol:propylene glycol and dosed at $6 \mu\text{l cm}^{-2}$ *trans*-cinnamaldehyde (99%, Sigma-Aldrich, Munich, Germany) was dissolved in 100% ethanol at 20% v/v and dosed topically at $50 \mu\text{l}$ dose volume.

Laser Doppler imaging protocol. Male Sprague Dawley rats were weighed and randomised to one of 2 treatment groups, placed in an anaesthetic chamber and anaesthetized with a 5% isoflurane/O₂ mix. Animals were then moved to a homeothermic heat mat and anaesthesia maintained at approximately 2% isoflurane/O₂ during the laser Doppler scanning *via* nose cone for the duration of the study. The abdomen was then shaved to allow laser Doppler flowmetry scans to be taken over an approximate area of 2.5 cm^2 . Baseline scans were recorded for 10 min, subsequently $15 \mu\text{l}$ of compound (50 mg ml^{-1} 4) or vehicle (70:30 ethanol:propylene glycol) will then be applied to the centre of the scan area. The treatment was left to penetrate the skin for 60 minutes while baseline blood flow was measured. After the treatment period, a further 5 post-dose Doppler scans were completed to establish a post-dose baseline before $50 \mu\text{l}$ of 20% *trans*-cinnamaldehyde (99%, Sigma-Aldrich, Munich, Germany) dissolved in 100% ethanol was administered topically to the centre of the scan area using a 12 mm polypropylene coated aluminium Finn chamber on Scanpor tape (Biodiagnostics Ltd, Worcestershire) applied for a 10 minute duration. The Finn chamber was removed and laser Doppler flowmetry scans were then recorded for 30 minutes.

Sample collection schedule. Terminal PK samples were taken from all animals *via* cardiac puncture at study endpoint (180 min post oral dose). Blood samples were centrifuged and resultant plasma samples were frozen at -20°C prior to bioanalysis.

Equipment and supplies list. MoorLDI2 laser Doppler imager (Moor Instruments Ltd, Axminster, UK).

Data analysis. All data design, randomization and analysis were handled in accordance with previous discussions with Non-Clinical Statistics group. In brief, area under the curve (AUC) analysis was carried out for normalized blood flow following cinnamaldehyde challenge. AUC values were then compared across groups using one-way ANOVA.

Plasmids and cell lines. Full-length human TRPA1 (hTRPA1)cDNA (Genbank accession Y10601) was cloned into inducible vector pcDNA5/TO (Invitrogen, Carlsbad, CA). DNA representing full-length opossum TRPA1 (oTRPA1, *Mono-delphis domestica* XP001378427) was codon-optimized, synthesized and cloned into pcDNA5/TO. The hS5 chimera was generated by gene synthesis of human S5 DNA which was cloned (using seamless cloning technology) into opossum TRPA1 to replace oS5. The oS5 chimera was generated by synthesis of opossum S5 DNA which was cloned into human TRPA1 to replace hS5. This resulted in a 27 amino acid swap such that for the hS5 chimera, hTRPA1 amino acids 867–893 replaced oTRPA1 amino acids 870–896. For the oS5 chimera,

oTRPA1 amino acids 870–896 replaced hTRPA1 amino acids 867–983. All gene synthesis and seamless cloning was performed by GenScript USA.

Stable clonal cell lines for each chimeric construct were generated by transfecting chimera plasmid DNA into 293-T-REx cell line (Invitrogen) and selecting with $150 \mu\text{g ml}^{-1}$ hygromycin and $5 \mu\text{g ml}^{-1}$ blasticidin (at 37°C with 10% CO₂). $1 \mu\text{g ml}^{-1}$ tetracycline was used to induce hTRPA1 expression for functional assays.

Whole-cell patch clamp electrophysiology. Whole-cell patch clamp recordings were obtained using patch pipettes with resistances of 1.5 to $3.0 \text{ M}\Omega$ when filled with the internal solution, consisting of (in mM) 90 CsCl, 32 CsF, 10 HEPES, 10 EGTA, 10 Cs₄ BAPTA, 1 MgCl₂, 5 Mg ATP, and 0.1 Na GTP, pH adjusted to 7.3 with CsOH. The external solution consisted of (in mM) 132 NaCl, 5.4 KCl, 1.8 CaCl₂, 0.8 MgCl₂, 10 HEPES, and 5 Glucose, pH adjusted to 7.4 with NaOH. To ensure complete dialysis with pipette solution, recordings began 1 min after establishment of whole-cell configuration. Subsequently, $150 \mu\text{M}$ cinnamaldehyde was perfused with the external solution to activate TRPA1 channels. Currents were recorded at room temperature with an Axopatch 200B amplifier and filtered at 1 kHz with a low-pass Bessel filter. Voltage protocols were elicited using Clampex 10.2 software and consisted of 150 ms. Depolarizing ramps from -40 mV followed by 100 ms steps to $+40 \text{ mV}$ and then to -40 mV repeated every 5 seconds from a holding potential of 15 mV . Currents were digitized using a Digidata 1440A data acquisition interface and analyzed using Clampfit 10.2 software. For these experiments the average steady state current at -40 mV was analyzed for each test condition. For potency experiments, cumulative concentration–responses were generated. Individual concentration–response relationships were fitted to a logistic equation with floating potency, slope and Emax. Individual concentration–relationships were then normalized to their fitted Emax to visualize all data on a single graph.

Acknowledgements

The authors would like to thank Neil Flanagan and Thean Yeoh for the skin flux and skin retention data.

Notes and references

- 1 Y. Kaneko and A. Szallasi, *Br. J. Pharmacol.*, 2014, **171**(10), 2474.
- 2 B. Nilius and A. Szallasi, *Pharmacol. Rev.*, 2014, **66**(3), 676.
- 3 (a) J. Chen, S. McGaraughty and P. R. Kym, in *TRP Channels in Drug Discovery: Volume 1*, ed. A. Szallasi and T. Biro, Humana Press, Springer Science + Business Media, 1st edn, 2012, ch. 3, pp. 43–59; (b) J. Chen and D. H. Hackos, *Naunyn Schmiedebergs Arch. Pharmacol.*, 2015, **388**, 451.
- 4 (a) S. E. Jordt, D. M. Bautista and H. H. Chuang, *Nature*, 2004, **427**, 260; (b) K. Talavera, M. Gees, Y. Karashima, V. M. Meseguer, J. A. Vanoirbeek, N. Damann, W. Everaerts, B. Wouter, M. Benoit, A. Janssens, R. Vennekens, F. Viana, N. Benoit, B. Nilius and T. Voets, *Nat. Neurosci.*, 2009, **12**, 1293.

- 5 (a) D. M. Bautista, S. E. Jordt, T. Nikai, P. R. Tsuruda, A. J. Read, J. Poblete, E. N. Yamoah, A. I. Basbaum and D. Julius, *Cell*, 2006, **124**, 1269; (b) U. Anand, W. R. Otto, P. Facer, N. Zebda, I. Selmer, M. J. Gunthorpe, I. P. Chessell, M. Sinisi, R. Birch and P. Anand, *Neurosci. Lett.*, 2008, **438**, 221.
- 6 B. Kremeyer, F. Lopera, J. J. Cox, A. Momin, F. Rugiero, S. Marsh, C. G. Woods, N. G. Jones, K. J. Paterson, F. R. Fricker, A. Villegas, N. Acosta, N. G. Tineda-Trujillo, J. D. Ramirez, J. Zea, M.-W. Burley, G. Bedoya, D. L. H. Bennett, J. N. Wood and A. Ruiz-Linares, *Neuron*, 2010, **66**, 671.
- 7 (a) S. McGaraughty, K. L. Chu, R. J. Perner, S. DiDomenico, M. E. Kort and P. R. Kym, *Mol. Pain*, 2010, **6**, 14; (b) J. Chen, S. K. Joshi, S. DiDomenico, R. J. Perner, J. P. Mikusa, D. M. Gauvin, J. A. Segreti, P. Han, X.-F. Zhang, W. Niforatos, B. R. Bianchi, S. J. Baker, C. Zhong, G. H. Simler, H. A. McDonald, R. G. Schmidt, S. P. McGaraughty, K. L. Chu, C. R. Faltynek, M. E. Kort, R. M. Reilly and P. R. Kym, *Pain*, 2011, **152**, 1165; (c) D. S. da Costa, F. C. Meotti, E. L. Andrade, P. C. Leal, E. M. Motta and J. B. Calixto, *Pain*, 2010, **148**, 431.
- 8 (a) K. Y. Kwan, A. J. Allchorne, M. A. Vollrath, A. P. Christensen, D.-S. Zhang, C. J. Woolf and D. P. Corey, *Neuron*, 2006, **50**, 277; (b) D. M. Bautista, P. Movahed, A. Hinman, H. E. Axelsson, O. Sterner, E. D. Hogestatt, D. Julius, S.-E. Jordt and P. E. Zygmunt, *Proc. Natl. Acad. Sci. U. S. A.*, 2005, **102**, 12248.
- 9 (a) D. M. Bautista, S. R. Wilson and M. A. Hoon, *Nat. Neurosci.*, 2014, **17**(2), 175; (b) S. R. Wilson, K. A. Gerhold, A. Bifolck-Fisher, Q. Liu, K. N. Patel, X. Dong and D. M. Bautista, *Nat. Neurosci.*, 2011, **14**(5), 595; (c) S. R. Wilson, L. The, L. M. Batia, K. Beattie, G. E. Katibah, S. P. McClain, M. Pellegrino, D. M. Estandian and D. M. Bautista, *Cell*, 2013, **155**, 285; (d) S. R. Wilson, A. M. Nelson, L. Batia, T. Morita, D. Estandian, D. M. Owens, E. A. Lumpkin and D. M. Bautista, *J. Neurosci.*, 2013, **33**(22), 9283.
- 10 (a) F. Cevikbas, X. Wang, T. Akiyama, C. Kempkes, T. Savinko, A. Antal, G. Kukova, T. Buhl, A. Ikoma, J. Buddenkotte, V. Soumelis, M. Feld, H. Alenius, S. R. Dillon, E. Carstens, B. Homey, A. Basbaum and M. Steinhoff, *J. Allergy Clin. Immunol.*, 2014, **133**(2), 448; (b) J. Liang, Q. Ji and W. Ji, *Neurosci. Lett.*, 2011, **492**(3), 175; (c) M. Kido-Nakahara, J. Buddenkotte, C. Kempkes, A. Ikoma, F. Cevikbas, T. Akiyama, F. Nunes, S. Seeliger, B. Hasdemir, C. Mess, T. Buhl, M. Sulk, F. U. Müller, D. Metze, N. W. Bunnett, A. Bhargava, E. Carstens, M. Furue and M. Steinhoff, *J. Clin. Invest.*, 2014, **124**(6), 2683.
- 11 T. L. Cvetkov, K. W. Huynh, M. R. Cohen and V. Y. Moiseenkova-Bell, *J. Biol. Chem.*, 2011, **286**, 38168.
- 12 C. E. Paulsen, J.-P. Armache, Y. Gao, Y. Chen and D. Julius, *Nature*, 2015, **520**, 511.
- 13 (a) L. J. MacPherson, X. Bailong, K. Y. Kwan, M. J. Petrus, A. E. Dubin, S. Hwang, B. Cravatt, D. P. Corey and A. Patapoutian, *J. Neurosci.*, 2007, **27**, 11412; (b) L. J. Macpherson, A. E. Dubin, M. J. Evans, F. Marr, P. G. Schultz, B. F. Cravatt and A. Patapoutian, *Nature*, 2007, **445**, 541.
- 14 (a) B. Xiao, A. E. Dubin, B. Bursulaya, V. Viswanath, T. J. Jegla and A. Patapoutian, *J. Neurosci.*, 2008, **28**(39), 9640; (b) M. Takaishi, K. Uchida, F. Fujita and M. Tominaga, *J. Physiol. Sci.*, 2014, **64**, 47; (c) G. Klement, L. Eisele, D. Malinowsky, A. Nolting, M. Svensson, G. Terp, D. Weigelt and M. Dabrowski, *Biophys. J.*, 2013, **104**, 798; (d) H. Moldenhauer, R. Latorre and J. Grandl, *PLoS One*, 2014, **9**, e106776.
- 15 (a) P. G. Baraldi, R. Romagnoli, G. Saponaro, M. A. Tabrizi, S. Baraldi, P. Pedretti, C. Fusi, R. Nassini, S. Materazzi, P. Geppetti and D. Preti, *Bioorg. Med. Chem.*, 2012, **20**, 1690; (b) K. S. A. Vallin, K. J. Sterky, E. Nyman, J. Bernstrom, R. From, C. Linde, A. B. E. Minidis, A. Nolting, K. Narhi, E. M. Santangelo, F. W. Sehgelmeble, D. Sohn, J. Strindlund and D. Weigelt, *Bioorg. Med. Chem.*, 2012, **22**, 5485; (c) G. Ortar, A. S. Moriello, E. Morera, M. Nalli, V. Di Marzo and L. De Petrocellis, *Bioorg. Med. Chem. Lett.*, 2013, **23**, 5614; (d) E. Morera, L. De Petrocellis, L. Morera, A. S. Moriello, M. Nalli, V. Di Marzo and G. Ortar, *Bioorg. Med. Chem. Lett.*, 2012, **22**, 1674; (e) P. G. Baraldi, D. Preti, S. Materazzi and P. Geppetti, *J. Med. Chem.*, 2010, **53**, 5085; (f) J.-D. Brederson, P. R. Kym and A. Szallasi, *Eur. J. Pharmacol.*, 2013, **716**, 61; (g) K. Salat, A. Moniczewski and T. Librowski, *Curr. Med. Chem.*, 2013, **20**, 1409; (h) A. M. Waskielewicz, A. Gunia, N. Szkaradek, K. Sloczynska, S. Krupinska and H. Marona, *Curr. Med. Chem.*, 2013, **20**, 1241; (i) L. Rooney, A. Vidal, A.-M. D-Souza, N. Devereux, B. Masick, V. Boissel, R. West, V. Head, R. Stringer, J. Lao, M. J. Petrus, A. Patapoutian, M. Nash, N. Stoakley, M. Panesar, J. M. Verkuy, A. M. Schumacher, H. M. Petrassi and D. C. Tully, *J. Med. Chem.*, 2014, **57**(12), 5129; (j) Y.-J. Hu, M. St-Onge, S. Laliberté, F. Vallee, S. Jin, L. Bedard, J. Labrecque and J. S. Albert, *Bioorg. Med. Chem. Lett.*, 2014, **24**(14), 3199; (k) S. Laliberté, F. Vallee, P.-A. Fournier, L. Bedard, J. Labrecque and J. S. Albert, *Bioorg. Med. Chem. Lett.*, 2014, **24**(14), 3204; (l) K. W. Copeland, A. A. Boezio, E. Cheung, J. Lee, P. Olivieri, L. B. Schenkel, Q. Wan, W. Wang, M. C. Wells, B. Youngblood, N. R. Gavva, S. G. Lehto and S. Geuns-Meyer, *Bioorg. Med. Chem. Lett.*, 2014, **24**(15), 3464; (m) L. B. Schenkel, P. Olivieri, A. A. Boezio, H. L. Deak, R. Emkey, R. F. Graceffa, H. Gunaydin, A. Guzman-Perez, J. H. Lee, Y. Teffera, W. Wang, B. D. Youngblood, V. L. Yu, M. Zhang, N. R. Gavva, S. G. Lehto and S. Geuns-Meyer, *J. Med. Chem.*, 2016, **69**(6), 2794.
- 16 (a) D. Preti, G. Saponaro and A. Szallasi, *Pharm. Pat. Anal.*, 2015, **4**(2), 75; (b) http://hydrabiosciences.com/pdf/press_releases/2012_01_10.pdf; (c) D. Preti, A. Szallasi and R. Patacchini, *Expert Opin. Ther. Pat.*, 2012, **22**(6), 663; (d) http://hydrabiosciences.com/pdf/press_releases/2015_04_14.pdf; (e) http://glenmarkpharma.com/GLN_NWS/news.aspx?res=P_GLN_NWS_RLS; (f) I. Mukhopadhyay, A. Kulkarni, S. Aranake, P. Karnik and M. Shetty, *PLoS One*, 2014, **9**(5), e97005, DOI: 10.1371/journal.pone.0097005; (g) Clinical Trials Gov. Clinical Trials Gov Identifier: NCT01726413. <http://clinicaltrials.gov>; (h) PR Newswire. *Glenmark's TRPA1 Antagonist 'GRC 17536' Shows Positive Data in a Proof of Concept Study* (2014), www.prnewswire.com.
- 17 L. Di, C. Whitney-Pickett, J. P. Umland, H. Zhang, X. Zhang, D. E. Gebhard, Y. Lai, J. J. Federico, R. E. Davidson, R. Smith, E. L. Reyner, C. Lee, B. Feng, C. Rotter, M. V. Varma,

- S. Kempshall, K. Fenner, A. F. El-Kattan, T. E. Liston and M. D. Troutman, *J. Pharm. Sci.*, 2011, **100**, 4974.
- 18 G. Allan, J. Davis, M. Dickins, I. Gardner, T. Jenkins, H. Jones, R. Webster and H. Westgate, *Xenobiotica*, 2008, **38**, 620.
- 19 Compounds were incubated at 10 μ M concentration with human liver microsomes for 15 min at 37 °C and the resulting samples analysed by LC-MS/UV to enable detection of drug-related material. The positive control incubations with verapamil formed the expected metabolites at appropriate levels in all cases.
- 20 pK_a values are calculated using an internal Pfizer pK_a calculation algorithm. Values ranged from pK_a 5.99 for 8 up to pK_a 8.57 for the bridged piperidine 34. Other values include 6.1 (30), 6.6 (31), 7.3 (32), 7.6 (35) and 7.98 (36).
- 21 S. R. Wilson, A. M. Nelson, L. Batia, T. Morita, D. Estandian, D. M. Owens, E. A. Lumpkin and D. M. Bautista, *J. Neurosci.*, 2013, **33**, 9283–9294; B. Liu, J. Escalera, S. Balakrishna, L. Fan, A. I. Caceres, E. Robinson, A. Sui, M. C. McKay, M. A. Alexander, C. A. Herrick and S. E. Jordt, *FASEB J.*, 2013, **27**, 3549.
- 22 A. I. Caceres, M. Brackmann, M. D. Elia, B. F. Bessac, D. del Camino, M. D'Amours, J. S. Witek, C. M. Fanger, J. A. Chong, N. J. Hayward, R. J. Homer, L. Cohn, X. Huang, M. M. Moran and S. E. Jordt, *Proc. Natl. Acad. Sci. U. S. A.*, 2009, **106**, 9099.
- 23 (a) N. Sharma, G. Agarwal, A. C. Rana, Z. Ali Bhat and D. Kumar, *Int. J. Drug Dev. Res.*, 2011, **3**(3), 70; (b) N. S. Chandrashekar and R. H. Shobha Rani, *Indian J. Pharm. Sci.*, 2008, **70**(1), 94.